Infrared cloud imaging in support of Earth-space optical communication

Paul W. Nugent,[1] Joseph A. Shaw,[1,*] and Sabino Piazzolla[2]

[1]*Department of Electrical and Computer Engineering, Montana State University, Bozeman, MT 59717, USA*
[2]*Optical Communications Group, Jet Propulsion Laboratory, 4800 Oak Grove Dr., M/S 161-135, Pasadena, CA 91109, USA*
**jshaw@montana.edu*

Abstract: The increasing need for high data return from near-Earth and deep-space missions is driving a demand for the establishment of Earth-space optical communication links. These links will require a nearly obstruction-free path to the communication platform, so there is a need to measure spatial and temporal statistics of clouds at potential ground-station sites. A technique is described that uses a ground-based thermal infrared imager to provide continuous day-night cloud detection and classification according to the cloud optical depth and potential communication channel attenuation. The benefit of retrieving cloud optical depth and corresponding attenuation is illustrated through measurements that identify cloudy times when optical communication may still be possible through thin clouds.

OCIS codes: (010.0280) Remote sensing and sensors; (010.1615) clouds; (110.3080) infrared imaging; (060.4510) optical communications; (010.5630) radiometry.

References and links

1. S. Piazzolla, S. Slobin, and P. E. Amini, "Cloud coverage diversity statistics for optical communication in the southwestern United States," JPL Publication **00–13** (2000).
2. M. Toyoshima, S. Yamakawa, T. Yamawaki, K. Arai, M. R. García-Talavera, A. Alonso, S. Sodnik, and B. Demelenne, "Long-term statistics of laser beam propagation in an optical ground-to-geostationary satellite communications link," IEEE Trans. Antenn. Propag. **53**(2), 842–850 (2005).
3. T. Jono, Y. Takayama, K. Shiratama, I. Mase, B. Demelenne, Z. Sodnik, A. Bird, M. Toyoshima, H. Kunimori, D. Giggenbach, N. Perlot, M. Knapek, and K. Arai, "Overview of the inter-orbit and orbit-to-ground laser communication demonstration by OICETS," Proc. SPIE **6457**, 645702 (2007).
4. F. Khatri, D. M. Boroson, D. V. Murphy, and J. Sharma, "Link analysis of Mars-Earth optical communications system," Proc. SPIE **5338**, 143–150 (2004).
5. J. A. Shaw, P. Nugent, N. J. Pust, B. Thurairajah, and K. Mizutani, "Radiometric cloud imaging with an uncooled microbolometer thermal infrared camera," Opt. Express **13**(15), 5807–5817 (2005), http://oe.osa.org/abstract.cfm?URI=oe-13-15-5807.
6. B. Thurairajah, and J. A. Shaw, "Cloud statistics measured with the infrared cloud imager (ICI)," IEEE Trans. Geosci. Remote Sens. **43**(9), 2000–2007 (2005).
7. P. W. Nugent, "*Wide-Angle Infrared Cloud Imager for Cloud Cover Statistics*," Masters Thesis, Electrical Engineering (Montana State University, 2008), *http://etd.lib.montana.edu/etd/2008/nugent/NugentP0508.pdf*.
8. J. H. Churnside and K. Shaik, "Atmospheric propagation issues relevant to optical communications," NOAA Technical Memorandum ERL WPL-159 (Jan. 1989).
9. G. L. Stephens, D. G. Vane, R. J. Boain, G. G. Mace, K. Sassen, Z. Wang, A. J. Illingworth, E. J. O'Connor, W. B. Rossow, S. L. Durden, S. D. Miller, R. T. Austin, A. Benedetti, C. Mitrescu, and the CloudSat Science Team, "The CloudSat mission and the A-Train,", Bull. Am. Met. Soc. **83**, 1771–1790 (2002).
10. G. P. Anderson, A. Berk, P. K. Acharya, M. W. Matthew, L. S. Bernstein, J. H. Chetwynd, H. Dothe, S. M. Adler-Golden, A. J. Ratkowski, G. W. Felde, J. A. Gardner, M. L. Hoke, S. C. Richtsmeier, B. Pukall, J. Mello, and L. S. Jeong, "MODTRAN4: radiative transfer modeling for remote sensing," Proc. SPIE **3866**, 2–10 (1999).
11. G. P. Anderson, S. A. Clough, F. X. Kneizys, J. H. Chetwynd, and E. P. Shettle, "AFGL atmospheric constituent profiles (0-120km)." Tech Report, Air Force Geophysics Laboratory Environmental Research Papers (1986).
12. J. A. Shaw, and L. Fedor, "Improved calibration of infrared radiometers for cloud-temperature remote sensing," Opt. Eng. **32**(5), 1002–1010 (1993).
13. E. Kassianov, C. N. Long, and M. Ovtchinnikov, "Cloud sky cover versus cloud fraction: whole-sky simulations and observations," J. Appl. Meteorol. **44**(1), 86–98 (2005).
14. T. Inoue, "A cloud type classification with NOAA 7 split-window measurements," J. Geophys. Res. **92**(D4), 3991–4000 (1987).

#102064 - $15.00 USD Received 29 Sep 2008; revised 15 Apr 2009; accepted 27 Apr 2009; published 28 Apr 2009

15. C. H. Reitan, "Surface dew point and water vapor aloft," J. Appl. Meteorol. **2**(6), 776–779 (1963).
16. C. Tomasi, "Determination of the total precipitable water vapor by varying the intercept in Reitan's relationship," J. Appl. Meteorol. **20**(9), 1058–1069 (1981).
17. K. Sassen, and G. G. Mace, "Ground-Based Remote Sensing of Cirrus Clouds," in *Cirrus*, D. K. Lynch, K. Sassen, D. O'C. Starr, and G. Stephens, eds (Oxford, New York, NY, 2002), pp 168–209.
18. J. A. Reagan, X. Wang, and M. T. Osborn, "Spaceborne lidar calibration from cirrus and molecular backscatter returns," IEEE Trans. Geosci. Rem. Sens. **40**(10), 2285–2290 (2002).

1. Introduction

The increasing demand for high-data-rate communication is generating interest in Earth-space optical links as an alternative or extension to radio-based links [1]. Optical links to both near-Earth and deep-space platforms are being studied by multiple organizations [1–4]. One of the key parameters of concern for Earth-space optical communication is cloud cover at the ground station [1]. Recently, the need to characterize clouds at optical communication ground sites with small, low-cost instruments led us to collaboratively develop a second-generation Infrared Cloud Imager (ICI2) system for continuous ground-based measurements of cloud cover statistics. The ICI2 builds on the first-generation ICI system that was developed for measuring clouds in climate studies [5,6], but offers much smaller size and lower cost.

The ICI systems are radiometrically calibrated, ground-based, long-wave infrared imagers based on uncooled microbolometer cameras that provide thermal images of the cloud base. In this technique, clouds are identified by observing thermal emission in the 8-13 μm atmospheric window, where cloud emission provides good radiometric contrast with the relatively low atmospheric emission [5,6]. The reliability of the ICI for cloud detection has been proven during deployments at multiple mid-latitude and Arctic sites through comparisons with co-located instruments, including microwave radiometers, cloud LIDARs and radars, and visible-wavelength cloud imagers [5,6]. The original ICI system has been demonstrated to measure cloud statistics in good agreement with lidars and radars and to provide improved consistency in detecting cloud during day and night relative to visible-wavelength imagers [6].

Two ICI2 systems are discussed in more detail in this paper, one with 62° diagonal field of view (fov) and one with 110° diagonal fov. Both systems have smaller size, lower cost and larger fov than the original ICI. All ICI systems identify and characterize clouds from sky radiance images after the clear-sky emission component has been estimated and removed. The ICI2 systems also use enhanced data processing algorithms for classifying the detected clouds quantitatively according to their optical depth (OD) and corresponding attenuation for a potential Earth-space optical communication channel.

The attenuation of an optical signal by clouds varies widely, depending on the cloud optical properties. Optically thick clouds attenuate the signal strongly enough to completely break the communication link. Optically thin clouds, in particular cirrus, attenuate the beam primarily through scattering, removing power from the signal path and degrading signal quality [8]. To fully characterize potential or existing Earth-space optical channels, accurate measurements of cloud presence and attenuation are required as a function of space and time.

Site selection for an optical ground station transceiver can be aided by the knowledge of statistical cloud cover at possible communication sites. Moreover, the link availability to a particular optical communication platform can be improved through the use of carefully selected multiple ground stations, or site diversity [1]. The selection of these sites requires knowledge of the localized long-term cloud cover with high temporal and spatial resolutions to enable calculation of site-diversity statistics and/or network availability. Optimal operation requires the local weather patterns of these locations, particularly local cloud cover, to be uncorrelated or anti-correlated at best [1]. Therefore, a statistical understanding of localized cloud cover at multiple locations is required in the development of a network of communication sites for Earth-space optical communication.

The requirements on an instrument to measure cloud cover in this application are the following: provide continuous data (day and night), contain both spatial and temporal data to characterize hourly, daily, and seasonal variability with zenith angle, and ideally provide real-

#102064 - $15.00 USD Received 29 Sep 2008; revised 15 Apr 2009; accepted 27 Apr 2009; published 28 Apr 2009

time cloud pattern data to allow for prediction of communication link availability. Thermal imaging from satellites can provide imagery of cloud tops with resolution on the order of km to tens of km per pixel [9], but these data may not always provide sufficiently high resolution to characterize the atmospheric paths of optical communication channels. However, a ground-based ICI can provide spatial resolution of 50 m or less for clouds at 10 km altitude.

In this paper we give an overview of the compact ICI2 systems, describe the cloud detection and classification techniques, and demonstrate the capabilities of these instruments for providing continuous day/night observation, detection, and classification of clouds. Data are shown that identify times when optical communication is likely possible through thin clouds, thereby illustrating the utility of the enhanced ICI2 cloud characterization capabilities relative to traditional cloud-presence detection.

2. Atmospheric effects in the longwave infrared window

The long-wave infrared window, approximately 8 μm to 13 μm, is well suited to observing clouds with an upward-viewing system because of relatively low absorption and emission. The two major sources of absorption or emission in this band are ozone centered at 9.6 μm and water vapor throughout. Thick clouds are easily detected in long-wave thermal infrared images because the cloud emission provides significant contrast relative to the generally low atmospheric emission. However, the radiometric contrast is much smaller for thin cirrus detection, which requires the atmospheric emission to be determined and removed for consistent detection with varying water vapor content.

Figure 1 shows that the low atmospheric absorption in the long-wave window leads to generally high atmospheric transmittance that is reduced by increasing water vapor. This figure depicts a MODTRAN-simulated transmittance spectrum for a zenith path from Bozeman, MT at 1.524 km above sea level (ASL) to space through the 1976 U.S. Standard Atmosphere (hereafter referred to as 76US) [10,11]. This plot is shown for two water vapor profiles: the default 76US profile (black line) and the default profile scaled by a factor of 1.5 (red line). The 1.5 × water vapor scale factor increases the precipitable water vapor (PWV) from 0.72 cm to 1.08 cm and the near-surface relative humidity from 51% to 76%.

Figure 2 shows a similar effect of variable water vapor, but in this case on the down-welling clear-sky thermal emission spectrum with three different water vapor profiles: zero water vapor (dotted black), default water vapor (blue), and 1.5 × default water vapor. The increased water vapor increases the background emission throughout the window region.

Figure 3 shows that the long-wave atmospheric emission is also increased by the presence of clouds. A clear-sky emission spectrum is shown as a reference, along with emission spectra for three cloud types: cirrus at 10 km ASL (1 km thick, OD = 1 at 550-nm); alto-stratus at 3.9 km ASL (0.6 km thick, OD = 77); and cumulus at 1.6 km ASL (2.6 km thick, OD = 241). Both liquid and ice clouds emit significant radiation throughout the window band, with nearly all liquid clouds and many thick ice clouds behaving as opaque black bodies [12]. While cumulus is easily detected, reliable detection of thin cirrus requires careful compensation of the clear-air emitted radiance component. This still leaves potential ambiguity in distinguishing between cirrus and optically thin fog or haze, but for the optical communication application it is most important to detect the presence of an attenuating layer, regardless of whether it is cirrus or fog. It may be possible to use a split-window technique to distinguish between thin liquid and ice clouds, but this also would reduce the available signal level (see related discussion in Section 3).

#102064 - $15.00 USD Received 29 Sep 2008; revised 15 Apr 2009; accepted 27 Apr 2009; published 28 Apr 2009

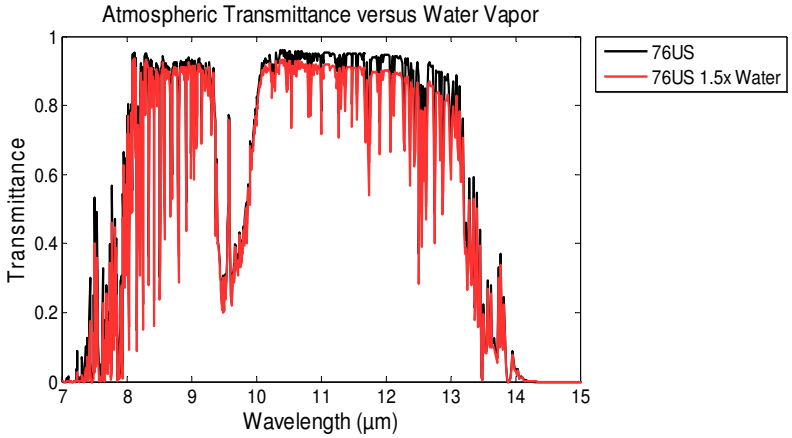

Fig. 1. MODTRAN-simulated transmittance for a zenith path through the 76US atmosphere (ground level 1.524 km ASL) with water vapor profiles using default (black) and 1.5 × default (red) values.

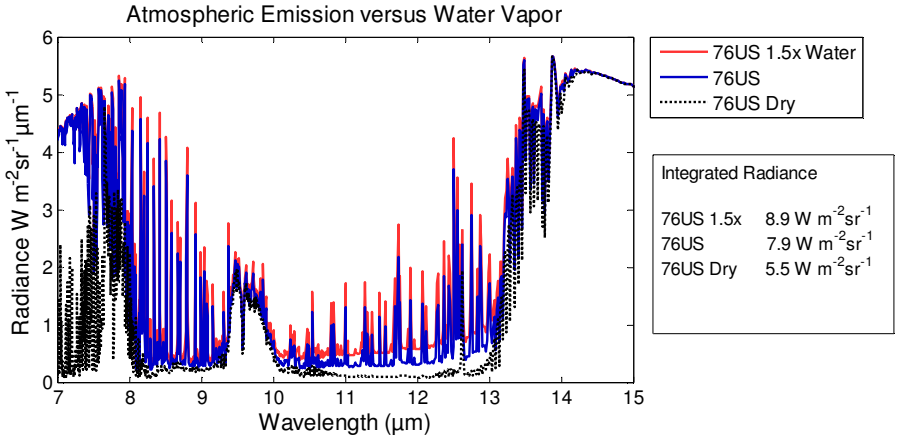

Fig. 2. MODTRAN down-welling atmospheric emission spectra for three cloud-free atmospheres: 76US with 1.5 × default water vapor (red, top), 76US default water vapor (blue, middle), and zero water vapor (dotted black, bottom).

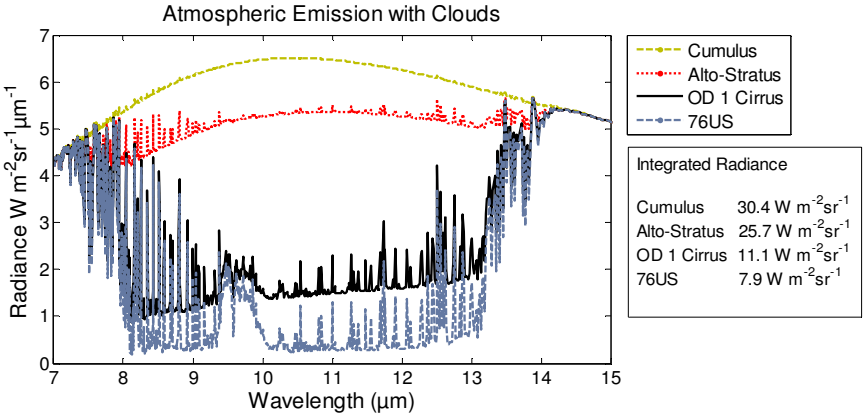

Fig. 3. MODTRAN down-welling emission for the 76US atmosphere with and without clouds: cumulus at 1.6 km ASL (gold dashed, top), altostratus at 3.9 km ASL (red dotted, middle), OD 1 cirrus at 10 km ASL (black, 2nd from bottom), and clear sky (blue dashed, bottom).

#102064 - $15.00 USD Received 29 Sep 2008; revised 15 Apr 2009; accepted 27 Apr 2009; published 28 Apr 2009

3. The compact second-generation Infrared Cloud Imager (ICI2)

The ICI2 instruments are much smaller, lower-cost versions of the original ICI [5,6]. The original ICI achieves higher sensitivity and stability through the use of a large-area blackbody reference source, but the smaller ICI2 is simpler to deploy and costs less. Data reported in this paper are from two compact ICI2 systems, one with a 50° × 38° (62° diagonal) field of view (fov), the other with a 86° × 67° (110° diagonal) fov. The 110° fov is close to the optimal value for comparing cloud fraction derived from ground-based and satellite sensors [13].

The Photon320 camera core, from Indigo Systems of FLIR Systems, Inc., was selected as the thermal imaging camera to be used in the ICI2 systems. This is a small, low-cost, thermal-infrared camera employing an uncooled microbolometer detector array that operates without a thermoelectric cooler (i.e., a TEC-less camera). The detector has 324 × 256 pixels. As indicated in Fig. 4, the compact ICI2 systems use an environmentally sealed enclosure to house the camera, a heater and associated control circuitry, a fan to circulate the internal air, a module to convert the Low Voltage Digital Signaling (LVDS) data to Ethernet signals for data acquisition and camera control, a hard carbon-coated germanium window through which the camera views the scene, and a baffle around the lens to shield the window from variable reflections of emission emanating from within the housing. The baffle improves the spatial uniformity of the window-dependent signal, but does not entirely remove the effects of the window. The algorithms developed to correct for these effects are described in a paper that is submitted but pending review at the time of this writing. Since the window-correction algorithms were not yet complete during early ICI2 measurements, the data presented here were taken with the window removed from the system.

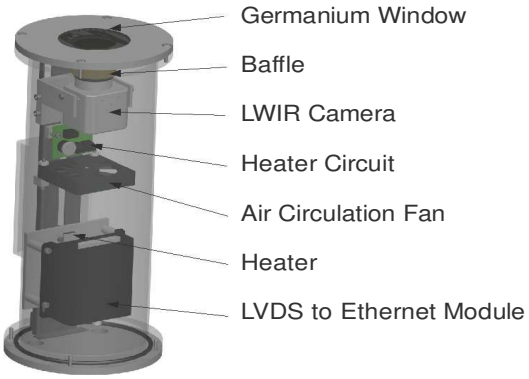

Fig. 4. An environmental enclosure houses the ICI2 system.

The ICI2 instruments are radiometrically calibrated to measure the band-integrated down-welling radiance ($W \cdot m^{-2} \cdot sr^{-1}$). This allows the removal of the radiance arising from atmospheric emission, thereby isolating the cloud signature [5,6]. Because the TEC-less microbolometer camera response drifts with temperature, software routines were developed to read the focal plane array temperature and provide real-time correction of the camera response. A unique set of routines are derived for each camera by operating it in a thermal chamber with varying temperature while viewing a constant-radiance blackbody source. This characterization provides a stable radiometric calibration that can be maintained without physical temperature stabilization. This provides a maximum calibration uncertainty of ± 0.44 $W \cdot m^{-2} \cdot sr^{-1}$ for the 62° fov system and ± 0.57 $W \cdot m^{-2} \cdot sr^{-1}$ for the 110° fov system (with no on-board blackbody). Referring to the band-integrated radiance values in Fig. 3, the 62° system's maximum calibration uncertainty is 5.5% of the 76US clear-sky emission, 4% of the cirrus emission, 1.7% of the altostratus emission, and 1.4% of the cumulus emission. Additional details of the calibration technique and uncertainty analysis are reported elsewhere [7].

The radiometric calibration and atmospheric emission removal algorithms also account for the low but measurable camera response on the edges of the atmospheric window [7]. For example, the camera's response is ~20% at 7.5 and 14.5 μm, where water vapor and CO2,

#102064 - $15.00 USD Received 29 Sep 2008; revised 15 Apr 2009; accepted 27 Apr 2009; published 28 Apr 2009

respectively, cause strong atmospheric emission (the 50% response wavelengths are 8.75 and 13.2 μm). Our calculations show that carefully selected narrow-bandpass filters can significantly reduce the sensitivity to non-cloud emission without excessively reducing the cloud signal, which is a step we plan for future ICI systems. This has the added benefit of reducing the temperature dependence of the atmospheric correction. It also may be possible to use a pair of narrow-band filters to enable split-window discrimination of thin liquid and ice clouds [14], but this would further reduce the optical bandwidth and make it more difficult to achieve adequate signal-to-noise ratio with uncooled microbolometer detectors. The use of cooled detectors would solve this problem, but also would significantly increase the cost and reduce the autonomous nature of the ICI systems.

4. Data processing

4.1 Atmospheric emission removal

The radiometrically calibrated measurements of down-welling sky radiance are processed in two steps to yield cloud presence and other cloud products. The first step is to remove the clear-sky atmospheric emission component, leaving a residual radiance or cloud-only emission. The second step is to apply one or more thresholds to the residual radiance to determine cloud presence and cloud optical depth or attenuation.

The routines used to remove the atmospheric emission rely on measurements of PWV and surface air temperature. These PWV and air temperature data are then used to calculate the emission expected from a clear sky in $W \cdot m^{-2} \cdot sr^{-1}$ [6,7]. The resulting clear-sky radiance value is subtracted from each pixel of the calibrated images to give a residual radiance that isolates cloud emission. The atmospheric emission removal algorithm also employs an angular correction that increases the PWV by the secant of the zenith angle for each pixel. This method estimates the atmospheric emission with an uncertainty less than ± 0.25 $W \cdot m^{-2} \cdot sr^{-1}$ at the outer edge of the widest field of view.

The required air temperature is readily available from surface meteorological stations and PWV measurements can be made with several sensors, including microwave radiometers, radiosondes, solar radiometers, and global positioning systems. Alternately, the PWV can be estimated through the Reitan Relationship using surface readings of dew-point and air temperature [15,16], but this inevitably increases the cloud-detection uncertainty.

4.2 Cloud detection and classification

Clouds are detected by applying a threshold-based algorithm to the residual radiance data after the background atmospheric emission is removed. This threshold is based on the combined uncertainty of the atmospheric correction and the camera calibrations, including a sufficient margin to prevent detecting spatial variations of water vapor as clouds.

In this paper, data are shown that were obtained with two different camera calibrations. The first calibration is for data taken before January 2008 (pre-08), and a second, improved, calibration is for data taken after January 2008 (08). The 08 calibration was developed using a blackbody with higher emissivity and less angular variation, but cannot be applied to earlier data owing to physical changes in the cameras. For these two calibrations, the minimum cloud-detection thresholds are as follows: 1 $W \cdot m^{-2} \cdot sr^{-1}$ for 08 data taken with either system (62° or 110° fov); 1.8 $W \cdot m^{-2} \cdot sr^{-1}$ for pre-08 data from the 110° fov system; and 2 $W \cdot m^{-2} \cdot sr^{-1}$ for pre-08 data from the 62° fov system. Although some older data shown here used the higher (i.e. less sensitive) threshold, all current data use the lower (more sensitive) threshold.

The ICI2 systems use a multi-threshold algorithm to classify the detected clouds according to their optical depth (OD) or the resulting optical-link attenuation. Without additional information, these algorithms actually provide an upper estimate of the cloud OD and only do so for the relatively thin clouds. Therefore, in this paper we classify clouds into bins of maximum OD at a wavelength of 550 nm according to the infrared cloud radiance calculated over the instrument bandwidth for cirrus clouds at 10 km altitude (or we can include lidar measurements of cloud height and a temperature profile to retrieve optical depth more

#102064 - $15.00 USD Received 29 Sep 2008; revised 15 Apr 2009; accepted 27 Apr 2009; published 28 Apr 2009

accurately). This method is applied only up to OD = 3 because thicker clouds behave as nearly ideal blackbodies [12,17] and thin clouds of OD ≤ 3 have a strong relationship between cloud OD and emissivity [17]. Therefore, emission from thin clouds depends strongly on cloud OD, allowing for OD classification from radiance measurements.

For the data presented here we used MODTRAN [10] to calculate the band-integrated infrared radiance for cirrus clouds at 10 km altitude for each of the OD-bin thresholds (e.g., OD = 0.15, 0.25, 1, and 3). The ICI2 measurements are grouped into bins of cloud radiance, which we interpret as bins of OD based on results of the MODTRAN simulations. Without further data on cloud height and temperature, we rely on bins of "OD < threshold value" rather than attempting to retrieve the actual OD. This method can result in some thin clouds being placed into the next higher bin; for example, a cloud with actual OD just less than 1 but located at a very low altitude (e.g. fog) may have a sufficiently high radiance (because of its warmer temperature relative to a 10-km cloud) to be counted in the OD < 3 bin instead of the OD < 1 bin. It is also possible to place some thin clouds into the next lower bin; for example, a cloud with actual OD just greater than 1 but located much higher than 10 km could have a sufficiently low radiance to be grouped into the OD < 1 bin instead of the OD < 3 bin. However, neither of these is a major concern because MODTRAN simulations show that the radiance depends much more strongly on OD than on temperature for very thin clouds. The ability of the ICI2 to provide cloud classification and cloud optical depth in addition to cloud presence increases the usefulness of this instrument in optical communication and climate research. Cloud optical depth is useful because it quantifies the extinction of an optical signal caused by a cloud. Table 1 shows the multi-level thresholds used in this study for cloud detection and classification for both the 62° fov and 110° fov ICI2 systems (note the improved minimum cloud detection threshold for the post-08 data).

For cirrus clouds, it can be assumed within a few percent that our derived 550-nm cloud OD (and corresponding attenuation loss in dB) is constant for potential communication wavelengths of 532 nm, 860 nm, 1064 nm, or 1550 nm. This is because the large size of cirrus ice crystals relative to the wavelength results in the optical properties of cirrus clouds changing very little over this spectral range [18].

Table 1. Cloud optical depth classification thresholds used in this paper. (For pre-08 data the "Very Thin" threshold fell into the undetectable range).

Cloud Description	Maximum Cloud OD @ 550 nm	Maximum Attenuation @ 550 nm	Cloud Detection Thresholds 110° fov Camera	Cloud Detection Thresholds 62° fov Camera
Undetectable	< 0.15	< 0.7 dB	< 1 $W \cdot m^{-2} \cdot sr^{-1}$	< 1 $W \cdot m^{-2} \cdot sr^{-1}$
1: Very Thin*	< 0.25	< 1.1 dB	1 - 1.8 $W \cdot m^{-2} \cdot sr^{-1}$	1 - 2.0 $W \cdot m^{-2} \cdot sr^{-1}$
2: Thin	< 1	< 4.3 dB	1.8 - 3.6 $W \cdot m^{-2} \cdot sr^{-1}$	2 - 4 $W \cdot m^{-2} \cdot sr^{-1}$
3: Mostly Thin	< 3	< 13 dB	3.6 -v5.5 $W \cdot m^{-2} \cdot sr^{-1}$	4 - 6 $W \cdot m^{-2} \cdot sr^{-1}$
4: Medium	> 3	> 13 dB	5.5 - 8 $W \cdot m^{-2} \cdot sr^{-1}$	6 - 9 $W \cdot m^{-2} \cdot sr^{-1}$
5: High-Level-Thick	High >> 3	High	8 - 12 $W \cdot m^{-2} \cdot sr^{-1}$	9 - 13 $W \cdot m^{-2} \cdot sr^{-1}$
6: Mid-Level-Thick	High >> 3	High	12 - 20 $W \cdot m^{-2} \cdot sr^{-1}$	13 - 22 $W \cdot m^{-2} \cdot sr^{-1}$
7:Low-Level Thick	High >> 3	High	> 20 $W \cdot m^{-2} \cdot sr^{-1}$	> 22 $W \cdot m^{-2} \cdot sr^{-1}$

5. Example data and results

In this section we show examples of ICI2 images and derived cloud presence and cloud OD. These data then are interpreted in terms of optical communication link availability.

5.1 Cloud spatial statistics

In Figs. 5-10 we show spatially processed cloud data from Bozeman MT. Figures 5-9 use the pre-08 calibration and Fig. 10 uses the improved 08 calibration. All cloud data shown here are presented in three-panel figures, for which the left panel is the calibrated sky radiance, the

#102064 - $15.00 USD Received 29 Sep 2008; revised 15 Apr 2009; accepted 27 Apr 2009; published 28 Apr 2009

center panel is the residual radiance remaining after removal of atmospheric emission, and the right panel is the cloud data product (in this case, cloud presence, OD, or attenuation).

Figures 5-7 show ICI2 images obtained in Bozeman, MT at 13:29 Mountain Standard Time (MST = UTC – 7 hours) with the 62° system (Figs. 5, 6) and the 110° fov system (Fig. 7). Whereas Fig. 5 shows simple cloud presence, the right panel of Fig. 6 shows the maximum OD for each pixel, revealing significant variation of cloud optical properties throughout the image. Figure 7 was recorded at the same time, but with the 110° fov ICI2 system, and processed to show cloud OD (compare with Fig. 6). Despite significantly different optics, the two cameras measure nearly identical cloud amounts and cloud OD over their common field of view (center portion of the images), providing added confidence in the calibrations.

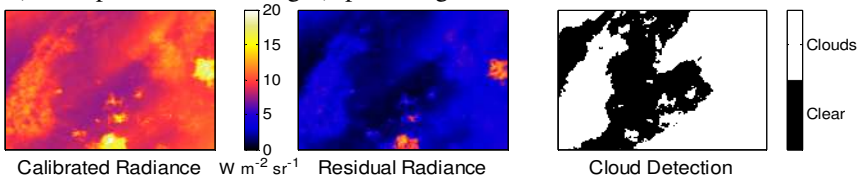

Fig. 5. ICI2 data measured at Bozeman, MT on 4 Oct. 2007 at 1329 MST (MST = UTC-7 hours). In this and subsequent 3-panel images, the left panel is the sky radiance image, the center panel is the residual radiance remaining after removal of clear-sky emission, and the right panel is the cloud product. In this figure the cloud product is cloud presence, with clouds shown in white and clear sky in black.

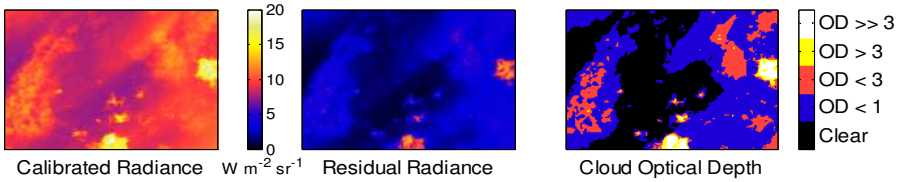

Fig. 6. Cloud OD data from the 62° system on 4 Oct. 2007 at 1329 MST.

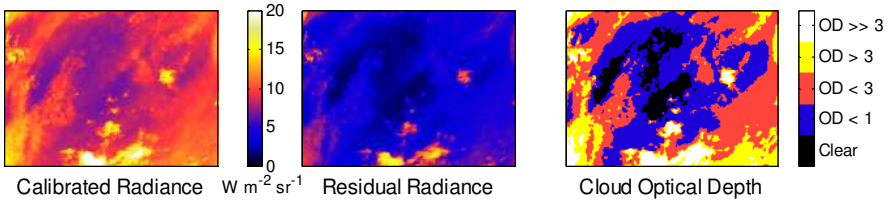

Fig. 7. Cloud OD data from the 110° fov system (compare with Fig. 6) on 4 Oct. 2007 at 1329 MST. The center portion of this image shows good agreement with the 62° image in Fig. 6.

Figures 8 and 9 show data from the 110° fov ICI2 system at two different times on 4 October 2007 with dramatically different conditions for a potential optical communication path. Figure 8 shows data from 10:13 MST for a nearly clear sky with only very thin cirrus clouds of optical depth less than 1. An optical communication link with a margin larger than 4.3 dB (OD = 1) should be able to operate through these clouds. This would be the case, for example, with a link margin of 7 dB as reported for a recent Earth-satellite optical propagation experiment [2].

Figure 9 shows data taken later the same day (13:49 MST on 4 Oct. 2007) after the conditions for communication had changed dramatically to cause a total blockage of nearly any optical link. In this image the sky is almost filled with thick clouds (OD>3) through which communication would not be possible.

#102064 - $15.00 USD Received 29 Sep 2008; revised 15 Apr 2009; accepted 27 Apr 2009; published 28 Apr 2009

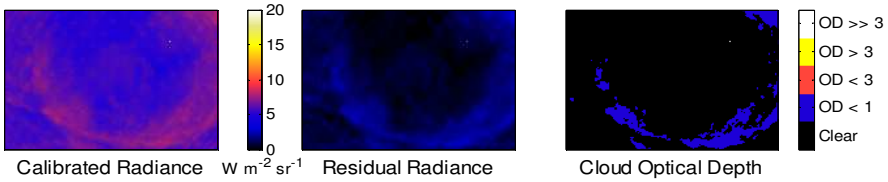

Fig. 8. Cloud optical depth data measured by the 110° fov ICI2 system for a mostly clear sky with thin cirrus clouds. The bright spot near the upper-right corner of the image is the Moon (algorithms are being developed to locate these pixels and prevent data errors from the sun or moon).

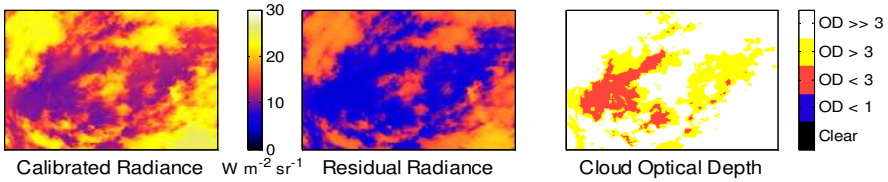

Fig. 9. Cloud OD data measured by the 110° fov ICI2 system for a fully overcast sky. There is a small portion of thinner clouds near the left center of the image with OD < 3 where optical communication may be possible for a short time.

Figure 10 shows data obtained at Bozeman, MT in March 2008 with a 62° fov ICI2 system using the improved 2008 calibration. Because of the improved calibration, the system is capable of accurately detecting clouds with a radiance threshold of 1.0 W/(m^2 sr^1), corresponding to OD < 0.25. The result is a finer gradation of OD on the color scale for Fig. 10 relative to the previous figures. All data obtained in 2008 and later provide the improved sensitivity to very thin clouds.

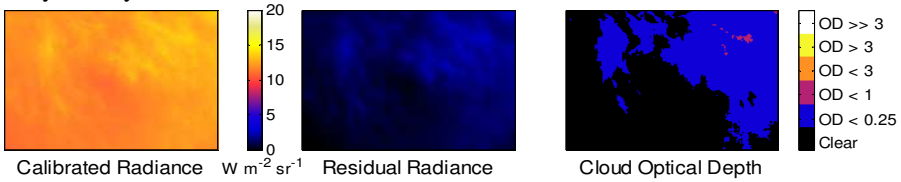

Fig. 10. Cloud optical depth data measured by a 62° fov ICI2 on 12 March 2008 at 13:41 MST for a sky that is partially filled with very thin clouds. An improved calibration provides increased sensitivity to thin clouds relative to previous figures, as indicated by the lower OD threshold in the color bar (note that a cloud with OD < 0.25 would cause 1.1 dB or less of attenuation).

The minimum cloud-detection threshold of 1 W·m^{-2}·sr^{-1}, OD < 0.25 at 10 km, or cloud attenuation less than 1.1 dB, is the current limitation of the ICI2 systems that operate without an on-board blackbody source. However, the ICI systems achieve higher sensitivity when operated with an onboard calibration source. Therefore, lower thin-cloud detection thresholds can be achieved with an infrared cloud imager system that includes an onboard blackbody calibration source at the expense of larger instrument size and increased cost. Work is continuing also on reducing cloud thresholds through improving the atmospheric emission correction routines (for example, taking into account the atmospheric emission changes that result when warm air overlies cold air in a temperature inversion).

5.2 Cloud Temporal Statistics

In addition to analyzing the spatial statistics of the data, a value of total cloud amount can also be computed from each image and analyzed as a time series. Total cloud amount is the percentage of cloud pixels across the entire fov. Using a multi-value cloud threshold, the detected clouds can be classified according to cloud optical depth, and cloud coverage statistics can be adapted to the requirements of Earth-space optical communication systems.

#102064 - $15.00 USD Received 29 Sep 2008; revised 15 Apr 2009; accepted 27 Apr 2009; published 28 Apr 2009

An example is shown in Fig. 11, which plots ICI2 measurements of the fraction of observed sky that is filled by clouds that generate loss below and above 7 dB. Although the choice of 7 dB as a threshold in Fig. 11 is purely arbitrary, in a general case one can consider this threshold as the link margin and therefore the statistics produced as the amount of time when the link was blocked by cloud attenuation. This link margin value can be related to an operational link budget, such as the one demonstrated during the Advanced Relay Technology Mission Satellite (ARTEMIS) transmission to a ground station in the Canary Islands [2]. Physically, the 7 dB loss can arise from a thin cloud of OD = 1.6 at 10 km altitude (MODTRAN-simulated cloud-only radiance = 5.4 $W \cdot m^{-2} \cdot sr^{-1}$ for the 76US atmosphere). The three curves in this plot indicate the fraction of the observed sky on 4 October 2007 filled with: all detected clouds; clouds with OD < 1.6 (attenuation < 7 dB); and clouds with OD > 1.6 (attenuation > 7 dB).

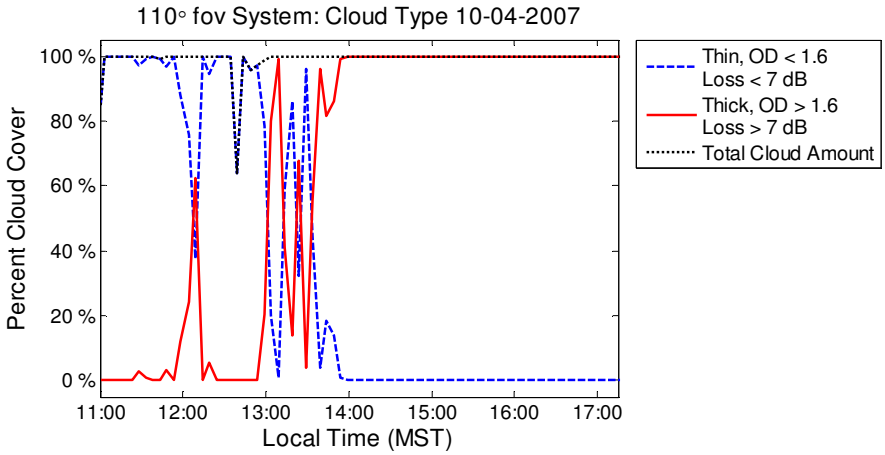

Fig. 11. Full-image cloud amount broken up into three categories: total cloudiness (dotted black line), thin clouds with OD < 1.6 or attenuation < 7 dB (dashed blue), and thick clouds with OD > 1.6 or attenuation > 7 dB (red line). Before approximately 13:00 MST communication may be possible, so simply detecting cloud presence, which leads to determination of a nearly constant 100% cloud amount, is insufficient to characterize the communication channel.

Figure 11 illustrates the importance of classifying clouds in optical depth bins. Although the total cloud amount is essentially constant at 100% throughout the day, aside from brief periods near 1200 and 1300 MST, this occurs with distinctly different types of clouds. Early in the day the sky has only thin clouds through which communication could be possible; later these are replaced by thicker clouds that would have blocked an optical communication signal. These clouds produce varying levels of operability for a hypothetical Earth-to-space communication channel based on the 7 dB link margin: from 11:00 MST to 13:00 MST communication would be possible 95% of the time; from 13:00 to 14:00 the reliability drops to only allowing communication 33% of the time; and after 14:00 the communication channel would be completely blocked.

This analysis demonstrates the utility of the cloud classification capabilities provided by the ICI systems. Simply detecting cloud presence is not sufficient to make an accurate analysis of the communication channel. In the example discussed here, three different levels of communication could occur with almost no change in the total cloud amount, which remains nearly 100% during the entire time period.

This is also similar to what was demonstrated with the Optical Inter-orbit Communication Engineering Test Satellite (OICETS) mission [3]. During this test, cloud cover was classified into clear, partly cloudy, cloudy, and rainy. Communication was successful always during clear and partly cloudy periods, never successful during rainy periods, but varied between success and failure during the cloudy periods. This provides further evidence that accurate

#102064 - $15.00 USD Received 29 Sep 2008; revised 15 Apr 2009; accepted 27 Apr 2009; published 28 Apr 2009

classification of cloud effects on an optical communication channel is best done with a system such as the ICI2 that is able to classify cloud cover in a manner that quantifies the optical extinction of the detected clouds with threshold levels that are easily adapted to fit the link margins of different communication links.

6. Discussion and conclusions

We have demonstrated the application of compact, ground-based, infrared cloud imagers for measuring spatial and temporal statistics of clouds and their optical effects on Earth-space optical communication links. The ICI2 systems described here are relatively small and low-cost thermal infrared cloud imagers that can be redeployed easily at multiple locations and can be reproduced with reasonably low cost. These imagers, however, require careful radiometric calibration. We illustrated how data from these imagers can be processed to generate maps of the spatial distribution of clouds, cloud optical depth and corresponding optical attenuation. This allows for classifying clouds according to the potential of maintaining optical communication through the clouds, with thresholds that are easily adaptable to a particular optical link margin.

Work is ongoing to improve the atmospheric emission removal algorithms, refine the cloud optical depth calculations by incorporating external data streams from sensors such as LIDARs or ceilometers, reduce sensitivity to atmospheric emission by using narrower spectral filters, and to perform long-term testing of the weatherproof system and its associated infrared window correction algorithms. These refinements will further reduce the calibration uncertainty of these systems and result in more accurate cloud detection, especially more sensitive detection of thin cirrus. The possibility of using a dual-band technique to more uniquely identify thin liquid and ice clouds has also being proposed.

We also have developed and currently are testing a third-generation ICI system (ICI3), which provides even higher sensitivity and improved calibration. This instrument uses the same camera and lens as the 110° ICI2, but also includes an on-board blackbody calibration source and an embedded micro-controller. Results of experiments being conducted to quantify this system's improved performance will be published in the near future.

Initial deployments of ICI2 systems at the NASA-JPL Table Mountain Facility, at Wrightwood CA, and at MSU have demonstrated their capability to measure clouds in a manner that is of immediate use to Earth-space optical communication studies. The application of thermal cloud imaging for the detection of clouds in support of Earth-space communication paths will be more fully demonstrated with a long-term deployment of these systems at the NASA-JPL Table Mountain Facility.

Acknowledgements

Portions of this research were carried out at the Jet Propulsion Laboratory, California Institute of Technology, under a contract with the National Aeronautics and Space Administration.

We gratefully acknowledge financial support provided by a Graduate Student Research Program fellowship through the NASA Stennis Space Center and use of a thermal chamber at the Montana State University Space Science and Engineering Laboratory.

#102064 - $15.00 USD Received 29 Sep 2008; revised 15 Apr 2009; accepted 27 Apr 2009; published 28 Apr 2009